energies

MDPI

Article

Effect of Selective Non-Catalytic Reduction Reaction on the Combustion and Emission Performance of In-Cylinder Direct Injection Diesel/Ammonia Dual Fuel Engines

Zhongcheng Wang *, Ruhong Li, Jie Zhu and Zhenqiang Fu

Merchat Marine College, Shanghai Maritime University, Shanghai 201306, China; 202330110121@stu.shmtu.edu.cn (R.L.); m19895436339@163.com (J.Z.); fuzhenqiangky@163.com (Z.F.)
* Correspondence: zcwang@shmtu.edu.cn

Abstract: Ammonia, as a hydrogen carrier and an ideal zero-carbon fuel, can be liquefied and stored under ambient temperature and pressure. Its application in internal combustion engines holds significant potential for promoting low-carbon emissions. However, due to its unique physicochemical properties, ammonia faces challenges in achieving ignition and combustion when used as a single fuel. Additionally, the presence of nitrogen atoms in ammonia results in increased NOx emissions in the exhaust. High-temperature selective non-catalytic reduction (SNCR) is an effective method for controlling flue gas emissions in engineering applications. By injecting ammonia as a NOx-reducing agent into exhaust gases at specific temperatures, NOx can be reduced to N_2, thereby directly lowering NOx concentrations within the cylinder. Based on this principle, a numerical simulation study was conducted to investigate two high-pressure injection strategies for sequential diesel/ammonia dual-fuel injection. By varying fuel spray orientations and injection durations, and adjusting the energy ratio between diesel and ammonia under different operating conditions, the combustion and emission characteristics of the engine were numerically analyzed. The results indicate that using in-cylinder high-pressure direct injection can maintain a constant total energy output while significantly reducing NOx emissions under high ammonia substitution ratios. This reduction is primarily attributed to the role of ammonia in forming NH_2, NH, and N radicals, which effectively reduce the dominant NO species in NOx. As the ammonia substitution ratio increases, CO_2 emissions are further reduced due to the absence of carbon atoms in ammonia. By adjusting the timing and duration of diesel and ammonia injection, tailpipe emissions can be effectively controlled, providing valuable insights into the development of diesel substitution fuels and exhaust emission control strategies.

Keywords: zero-carbon fuel; high temperature selective non-catalytic reduction; diesel ignition; engine emission characteristics

Academic Editor: Constantine D. Rakopoulos

Received: 6 December 2024
Revised: 21 January 2025
Accepted: 23 January 2025
Published: 25 January 2025

Citation: Wang, Z.; Li, R.; Zhu, J.; Fu, Z. Effect of Selective Non-Catalytic Reduction Reaction on the Combustion and Emission Performance of In-Cylinder Direct Injection Diesel/Ammonia Dual Fuel Engines. *Energies* **2025**, *18*, 565. https://doi.org/10.3390/en18030565

1. Introduction

Ammonia (NH_3), as a zero-carbon fuel, benefits from a well-established production process. Compared to hydrogen, another zero-carbon fuel, ammonia offers advantages such as higher energy density and easier storage and transportation. However, its high auto-ignition temperature and low laminar flame speed present challenges in terms of combustion heat release and emission control in engines. Currently, there are two main

methods for achieving ammonia combustion in diesel engines: 1. Introducing ammonia through the intake manifold, where it forms a combustible mixture with air during the intake valve lift before entering the cylinder. 2. Directly injecting ammonia into a high-pressure liquid state into the cylinder. However, achieving compression ignition with pure ammonia using direct injection is difficult. Therefore, auxiliary fuels or ignition methods are required to facilitate the combustion process and enable ammonia's diffusion of combustion and heat release [1–4].

Li et al. [5] compared the combustion and emission characteristics of dual-fuel low-pressure and high-pressure injection modes. The results showed that high-pressure direct injection enables a higher ammonia substitution ratio and reduces NOx emissions and ammonia slip while maintaining a thermal efficiency similar to pure diesel. Stephanie Frankl et al. [6] conducted numerical studies on high-pressure dual-fuel direct injection of ammonia, demonstrating that ammonia can burn efficiently and stably under high-pressure injection. Higher injection pressures and fuel temperatures positively impact thermal efficiency. According to the studies by Reiter and Kong [7,8], using ammonia introduced through the intake port and ignited by diesel while maintaining the original diesel injection system resulted in overall thermal efficiencies of 33–38% when ammonia's energy substitution ratio was 40–80%. However, at a 95% substitution ratio, the efficiency dropped to 19%. Compared to pure diesel combustion, premixed combustion with ammonia significantly increases hydrocarbon and carbon monoxide emissions, while higher ammonia substitution rates further increase NOx emissions. Zhang et al. [9] used numerical simulations to study high-pressure direct injection (HPDI) of liquid ammonia in a four-stroke engine, comparing the combustion and emission characteristics under varying ammonia ratios, injection timings, and spray orientations. The results indicated that liquid ammonia HPDI alters the combustion mode, improves fuel–air mixing, achieves more complete combustion, and significantly reduces greenhouse gas emissions compared to pure diesel mode. Yang et al. [10] investigated high-pressure direct injection post-injection strategies for diesel/ammonia dual-fuel combustion. Their findings revealed that optimizing the post-injection timing could reduce NOx emissions. Nevertheless, higher thermal efficiency is inevitably accompanied by increased NOx emissions, particularly in liquid ammonia combustion, where the nitrogen atoms in ammonia contribute to significant fuel-based and thermal NOx formation. Existing studies indicate that high-pressure injection strategies can achieve high ammonia substitution ratios while significantly lowering NOx emissions.

NOx reduction technologies include internal reduction methods and external exhaust after-treatment. Most research focuses on selective catalytic reduction (SCR) technologies for post-exhaust treatment, where additives can be supplemented under certain conditions to aid the reduction process. In contrast, selective non-catalytic reduction (SNCR) technology applied within the engine cylinder remains in the theoretical stage. This study uses numerical simulation to investigate the effects of dual direct injection of diesel and ammonia on combustion and emissions. Key engine performance parameters, such as cylinder pressure, temperature, and heat release rate, as well as the total generation of NOx emissions, were analyzed under various blending ratios and injection sequencing strategies.

2. Methodology

2.1. Model Establishment

The MAN L23/30H engine was selected as the research object, with its key structural parameters listed in Table 1. Based on the piston geometry, the sector module in the CONVERGE software was used to extract the piston's geometric profile and reconstruct the combustion chamber model. Since the combustion chamber exhibits axial symmetry

and the eight spray holes are uniformly distributed, a 1/8 sector model was adopted to simplify the simulation and conserve computational resources. In this study, a dual-nozzle in-cylinder direct injection strategy was employed to organize fuel combustion. Referring to the dual-fuel injection strategy achieved in [11], which combines diesel with low-carbon fuels, the spray cone angles for diesel and ammonia were configured to overlap in a staggered manner. In the XY plane, the interval angle 'α' between the diesel and ammonia sprays was set to 22.5°, ensuring a centrally symmetric and uniform fuel spray distribution after coupling on the full model. In the XZ plane, the diesel spray tilt angle was set to 70°, while the ammonia spray tilt angle was 65°, with an interval angle 'β' of 5°. Both the diesel and ammonia spray cone angles were set to 14°. The resulting simulation model at the top dead center (TDC) is shown in Figure 1. The chemical reaction mechanism used in this study is the multi-component mechanism proposed by Xu [12], consisting of 69 species and 389 elementary reactions. This mechanism has been validated for simulating the blending combustion process in diesel/ammonia dual-fuel engines.

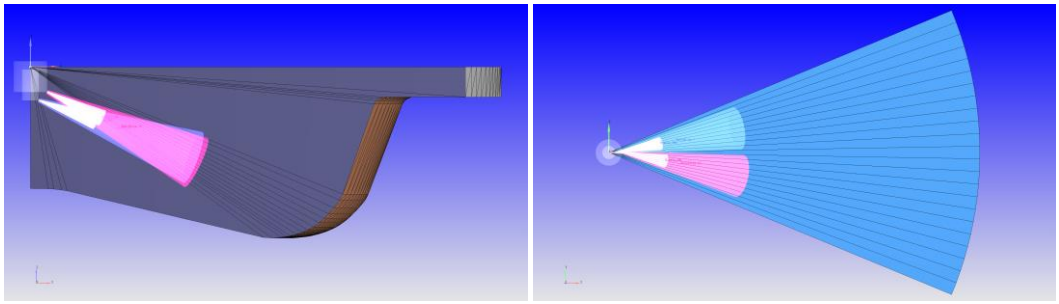

Figure 1. Geometric model of the engine cylinder (XZ plane and XY plane).

Table 1. Main structural parameters of MAN L23H30 single-cylinder diesel engine.

The Parameter Name	Parameter Values
Bore×Stroke/mm × mm	225 × 300
Connecting rod/mm	600
Speed (r/min)	900
Cylinder displacement/L	11.9
Compression ratio	13.5

2.2. Simulation Submodel Settings

The turbulent parameters at the valve opening timing were adjusted based on the engine's structural parameters. The combustion chamber turbulence was solved using the Reynolds-Averaged Navier–Stokes (RANS) method in conjunction with the RNG *k-ε* turbulence model [13]. The Kelvin–Helmholtz Rayleigh–Taylor (KH-RT) model was employed for droplet breakup, with submodel parameters referenced from the spray droplet breakup settings of Shi et al. [14]. Specific parameter values are listed in Table 2. The Frossling model was used to simulate droplet evaporation, while the NTC model was applied for droplet collision. Combustion was modeled using the SAGE model, which allows for selecting the appropriate chemical mechanisms and thermophysical property files based on simulation requirements. The SAGE model was activated from the start of fuel injection until the end of combustion. The selection of other submodels used in the simulation is summarized in Table 3.

Redefine the in-cylinder turbulence parameters according to the engine parameters and estimate the turbulence kinetic energy from

$$k_{init} = \frac{3}{2} \cdot (v')^2 \quad (1)$$

Specify the turbulence length scale as

$$l_{init} = 0.025 \cdot bore \quad (2)$$

Calculate the turbulence dissipation rate from

$$\varepsilon_{init} = C_{\mu}^{3/4} \cdot \frac{k_{init}^{3/2}}{l_{init}} \quad (3)$$

Table 2. Settings of parameter of KH-RT model.

Submodel	Parameter Values	Diesel Spray Model	Ammonia Spray Model
KH-model	Size constant B_0	0.61	0.61
	Velocity constant C_1	0.188	0.188
	Breakup time constant B_1	0.1	8.0
RT-model	Breakup time constant C_τ	1.5	0.95
	Size constant C_{RT}	0.5	0.4

Table 3. Selection of simulation submodel.

Physical Model Name	Submodel Settings
Turbulence model	RNG k-ε [15]
Spray breakup model	KH-RT [16]
Drop turbulent dispersion model	Wall Film-O'Rourke [17]
Spray collision model	NTC collision [18]
Wall heat transfer model	Han and Reitz model [19]
Combustion model	SAGE [20]
Carbon smoke emission model	Hiroyasu soot [21]
NOx formation model	Extended Zeldovich [22]

2.3. Simulation Model Calibration

CONVERGE offers three main grid control methods: Base Grid, Adaptive Mesh Refinement (AMR), and Fixed Embedding. AMR refines the grid dynamically based on velocity, temperature, and species fields, allowing customization of refinement levels and durations. Fixed embedding enables localized mesh refinement for specific regions, such as the nozzle, piston, and near-wall boundary layers. These refinement methods operate independently, allowing users to customize refinement time and levels as needed, and they can be executed in parallel to achieve precise grid size control. In this study, the engine and simulation model validation were based on experimental results obtained from the original engine operating in a single-fuel diesel mode. Four base grid sizes were tested in the simulation: 8 mm, 6 mm, 4 mm, and 2 mm. Using a 4 mm base grid, the boundary layer was refined with a two-level AMR strategy, while the fuel spray region was refined with a three-level fixed embedding strategy. Near the top dead center (TDC), the refined spray and wall mesh regions are shown in Figure 2.

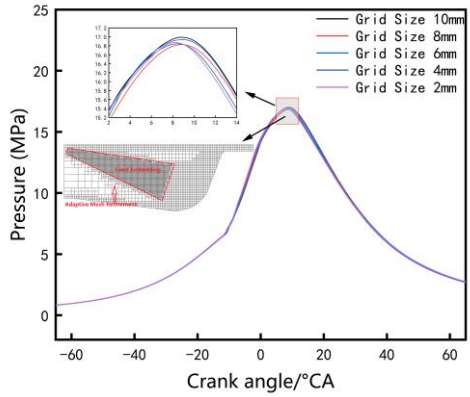

Figure 2. Grid division strategy.

The simulation data were provided by Zhenjiang CSSC Marine Power Co., Ltd. (Zhenjiang, China) The in-cylinder average pressure curve obtained from engine performance experiments was used to validate the simulation model. As shown in Figure 3, under standard operating conditions (engine speed: 900 rpm, fuel injection mass: 1.25 g, injection timing: −5 °CA), the simulation results closely matched the experimental data, with minimal error and good agreement in the inflection points of the pressure rise curves. Therefore, the reconstructed combustion chamber model, based on engine structural parameters and reasonable grid settings, is suitable for further simulation studies. Considering the trade-off between computational accuracy and resource limitations, a base grid size of 4 mm was selected for all simulation cases and operating conditions.

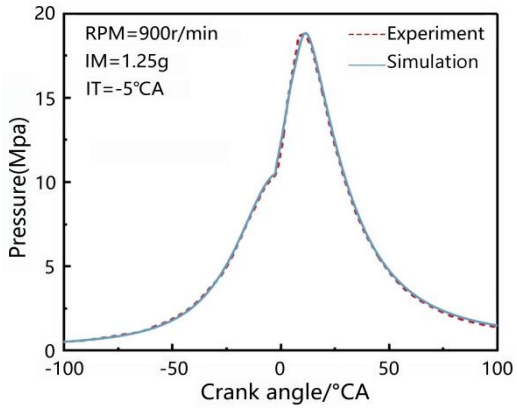

Figure 3. Simulation model calibration.

2.4. Mechanism Analysis of NOx Reduction

Ideally, the combustion products of ammonia would consist solely of water and nitrogen gas. However, when ammonia serves as the primary fuel in dual-fuel engines—particularly when the ammonia energy substitution exceeds 50%—it dominates the combustion process, leading to substantial nitrogen oxide (NOx) emissions. Thus, it is necessary to analyze the reaction pathways leading to NOx formation during ammonia combustion. As shown in Figure 4, the NOx formation process in ammonia-fueled engines is closely linked to the dehydrogenation and oxidation reactions that occur as combustion progresses. The dehydrogenation of ammonia is a key pathway during ignition and combustion, primarily involving its reaction with OH radicals. The first reaction to occur is $NH_3 = NH_2 + H$ [23,24]. Subsequently, under the influence of radicals such as OH and O, further reactions occur, including $NH_3 + OH = NH_2 + H_2O$ and $NH_3 + O = NH_2 + OH$, with NH_3 continuously losing hydrogen atoms [25,26]. The intermediates NH_i (i = 0, 1, 2)

are either directly oxidized or converted to NOx through intermediate species such as HNO and H_2NO under the influence of O, O_2, and OH [27,28]. HNO plays a crucial role in NO formation, while the concentrations of radicals such as O, O_2, and OH impact the oxidation process [29,30]. The reduction of NOx primarily occurs through reactions between NH_i and NO, which depend on the temperature of the reaction environment. Polymerization reactions involve the combination of NH_i radicals and the interconversion of their reaction products [31,32]. Through these pathways, the ammonia fuel eventually forms N_2 and NO, while NO can also convert to N_2 via key intermediate steps [33,34].

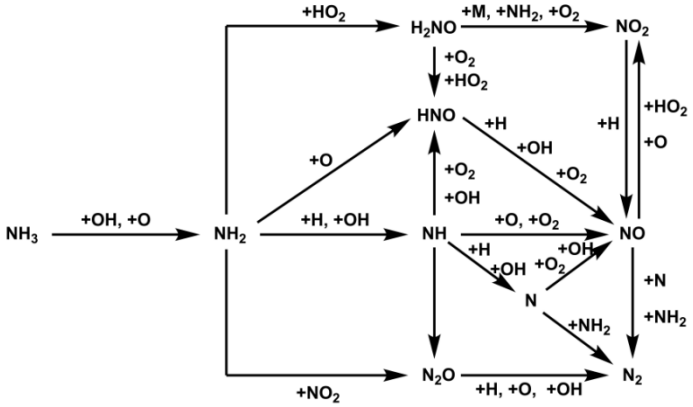

Figure 4. Main reaction pathway of ammonia oxidation.

2.5. Simulation Scheme Setting

At the rated operating conditions, the engine speed was 900 rpm. Two comparison scenarios, Case 1 and Case 2, were set based on the sequence of diesel and ammonia fuel injection. In Case 1, diesel is injected first, followed by ammonia fuel injection. In Case 2, a portion of ammonia is injected first, forming a partially homogeneous premixed gas with ammonia and air. During diesel injection, ammonia injection continues. Both scenarios set the ammonia fuel blending ratio from 10% to 90%, with a total of 18 operating conditions for comparison. In both scenarios, diesel not only serves as the fuel but also plays an ignition role during dual-fuel combustion. The original engine parameter for injection timing is set to 5° BTDC, and the nozzle diameter of the diesel injector is 0.33 mm. In the simulation scenarios of Case 1 and Case 2, both fuels are injected using a high-pressure injection strategy. Due to the distinct physicochemical properties of ammonia compared to diesel, even when the ammonia nozzle diameter is increased to 0.4 mm, and the injection pressure is set to match that of the diesel injector, ammonia fuel still requires a long injection duration in all scenarios. The time span for fuel entering the cylinder will be very long. To ensure that the various fuels can successfully enter the cylinder for combustion, in Case 1, the diesel injection timing is fixed at 14.5° BTDC, and the ammonia injection timing is fixed with a delay of 3 °CA. In Case 2, the ammonia injection timing is fixed at 15° BTDC, and the diesel injection timing is set sequentially with delays of 5 °CA, 8 °CA, and 10 °CA based on the ammonia substitution rate, ensuring that there is enough diesel fuel for ignition when the piston reaches the top dead center. The injection pressure for both fuels is set to 100 MPa. The ammonia substitution rate, denoted as R_{NH3}, is defined as the percentage of the ammonia fuel heating value relative to the total heating value of all fuel injected into the cylinder for the given operating condition. The calculation formula is:

$$R_{NH3} = \frac{M_{NH3} \times LHV_{NH3}}{M_D \times LHV_D + M_{NH3} \times LHV_{NH3}} \times 100\% \quad (4)$$

The computational model does not consider the intake and exhaust processes, thus eliminating the need to account for factors such as valve lift. The simulation process starts at the intake valve closing timing of −156 °CA and ends at the exhaust valve opening timing of 126 °CA. The boundary conditions are listed in Table 4.

Table 4. Simulation parameters under calibration conditions.

Items	Parameter Values
Initial pressure (bar)	2.3
Initial temperature (K)	365
Piston temperature (K)	550
Cylinder wall temperature (K)	470
Cylinder head temperature (K)	520

3. Results and Discussions

3.1. Effect of Different Mixing Ratios on Engine Combustion Performance

Compared to the original engine's pure diesel combustion mode, the cylinder pressure of each operating condition changed when ammonia was used to replace a portion of the diesel. The main factor behind this change was the new liquid ammonia high-pressure direct injection strategy, which altered the original combustion mode, as shown in Figure 5. To ensure that the total heat output for each operating condition in both scenarios remained constant for comparison, the injection pressures of diesel and ammonia and the total input heating value remained unchanged. As the ammonia substitution rate increased, the amount of diesel fuel decreased accordingly, and the diesel injection duration gradually shortened while the liquid ammonia injection duration increased. In Case 1, the diesel injection start timing and the liquid ammonia injection start timing were fixed (−14.5 °CA; −11.5 °CA). At lower ammonia substitution rates, the total injection time required for both fuels was shorter, and the overlap time between the two fuel injections first increased and then decreased. This led to more concentrated combustion and higher peak values for the average cylinder pressure curve. When the ammonia substitution rate was below 70%, the engine IMEP (mean effective pressure) increased. In particular, at a 40% ammonia substitution rate, the cylinder pressure peak was the highest, with an increase of 2.68 MPa compared to the original engine model. As the ammonia substitution rate continued to increase, the cylinder pressure peak started to drop. At a 70% ammonia substitution rate, the cylinder pressure peak was almost the same as that of the original engine model. After exceeding a 70% ammonia substitution rate, the cylinder pressure started to decrease due to the prolonged fuel injection time and the resulting less concentrated combustion. At the 80% and 90% ammonia substitution rate conditions, the cylinder pressure peaks decreased by 1.28 MPa and 2.7 MPa, respectively. In Case 2, the diesel injection start timing was appropriately adjusted. The liquid ammonia injected first mixed with air inside the cylinder to form a homogeneous combustible gas. The cylinder pressure peak increased at lower ammonia substitution rates, and as the diesel injection timing was gradually delayed with an increasing substitution rate, the inflection point of the cylinder pressure curve was also delayed. At high ammonia substitution rates, the cylinder pressure peak gradually decreased due to combustion being less concentrated, caused by the prolonged fuel injection time and the fuel's combustion characteristics. Similarly, at a 40% ammonia substitution rate, compared to the original engine model, the cylinder pressure peak increased by 1.9 MPa, and at the 80% and 90% substitution rates, the cylinder pressure peaks decreased by 0.23 MPa and 1.95 MPa, respectively.

Based on the sequence of diesel and ammonia injection, in Case 1, the strategy was to inject diesel first, followed by ammonia after an equal crank angle interval. The high-temperature heat source generated by diesel ignited the ammonia fuel. As the ammonia substitution rate increased, the diesel injection duration shortened, and the ammonia injection duration increased. According to ammonia combustion characteristics, at high ammonia substitution rates, the heat release rate curve exhibited a second prolonged peak after the first peak. The combustion process inside the cylinder could be divided into two stages: diesel diffusion combustion and ammonia fuel diffusion combustion. According to the heat release rate curve trend in Case 2, ammonia as a single fuel cannot achieve ignition combustion by itself when entering the cylinder. In this scenario, ignition combustion of the fuel in each operating condition still required the subsequent injection of diesel. The difference was that ammonia fuel, entering the cylinder first, formed a large amount of premixed combustible gas with the air inside the cylinder. Once the diesel fuel entered the cylinder, the ammonia fuel ignited, and the flame spread rapidly. Therefore, in Case 2, the combustion process of ammonia fuel consisted of two stages: ammonia premixed combustion and ammonia diffusion combustion, with the heat release rate curve resembling a partially premixed characteristic.

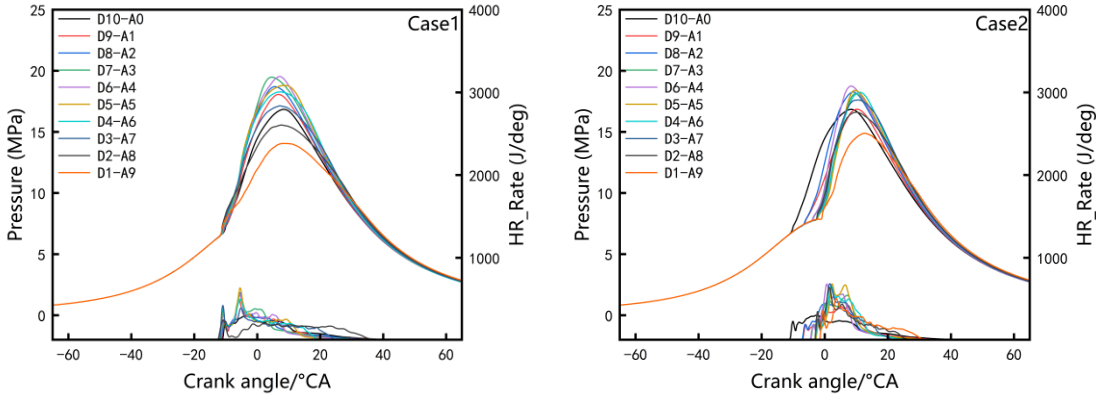

Figure 5. Changes in the cylinder pressure and heat release rate of different diesel/ammonia ratios under the two injection schemes.

CA10 and CA50 are defined as the crank angle positions at which the cumulative heat release reaches 10% and 50% of the total heat release, respectively. The combustion duration is the time interval between the CA10 and CA90 positions. As shown in Figure 6, in Case 1, with the increase in the ammonia substitution rate, both the CA50 position and combustion duration initially advanced and then delayed. This is because, at low ammonia substitution rates, ammonia accounted for a smaller proportion of the total fuel energy. Additionally, the dual-fuel injection strategy resulted in the ammonia injection duration being included within the diesel injection duration at low ammonia substitution rates, significantly reducing the overall injection time. The ammonia fuel burns faster, so CA50 occurred earlier. At moderate ammonia substitution rates, although the mass and injection duration of ammonia fuel gradually increased, the duration of dual-fuel injection also lengthened, and it occupied more than half of the ammonia injection duration, so CA50 continued to advance. After the ammonia substitution rate exceeded 50%, due to the nozzle diameter setting and the physicochemical properties of liquid ammonia droplets, the ammonia injection duration exceeded the diesel injection duration and gradually became the dominant fuel for combustion. The CA50 position was gradually delayed. Because Case 1 fixed the injection start time for both fuels, the variation in CA10 was minimal. Combined with the low flammability of ammonia fuel, the overall combustion duration gradually extended. In Case 2, the ammonia injection start time was

fixed, and the diesel injection time was delayed with the increasing ammonia substitution rate, gradually approaching the top dead center (TDC). Therefore, the CA10 time was also gradually delayed. Since single ammonia fuel cannot achieve ignition combustion under the compression ratio and wall temperature conditions of this engine model, the changes in CA50 and combustion duration at low substitution rates were mainly determined by the diesel injection settings. In conditions where the ammonia substitution rate was less than 50%, the total fuel injection duration was shorter than that of the original engine model, and the CA50 and combustion duration were slightly advanced and shortened. At higher ammonia substitution rates, CA50 and combustion duration gradually delayed and extended.

Both scenarios show the phenomenon where, at low ammonia substitution rates, CA50 and combustion duration advanced and shortened. This is because the dual-fuel injection strategy makes the small amount of liquid ammonia more effective in promoting combustion, thus shortening the combustion duration. However, at high ammonia substitution rates, the slower combustion speed of ammonia had a greater impact on the overall fuel combustion. In both cases, the combustion duration gradually lengthened. This is because the amount of diesel injected into the cylinder decreases as the ammonia energy replacement ratio increases. After the diesel injection and combustion were completed, the remaining ammonia fuel in the cylinder lacked a source of ignition, and because the ammonia flame propagation speed was slow, it was difficult to achieve complete combustion by its own flame propagation. Furthermore, at high ammonia substitution rates, there may be misfires in the later stages of combustion.

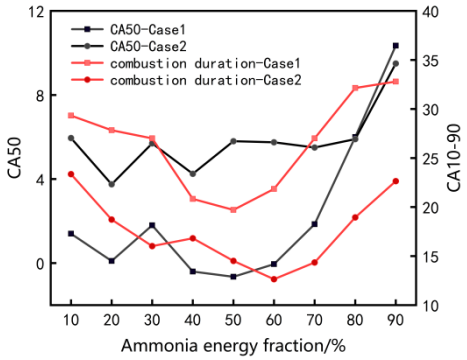

Figure 6. Effect of different diesel/ammonia ratios on CA50 and combustion duration under the two injection schemes.

3.2. In-Cylinder Temperature Analysis

After adopting the high-pressure direct injection fuel strategy at low ammonia substitution rates, the engine's in-cylinder temperature increased. This is primarily because this injection method improves the fuel–air mixing, accelerating the combustion speed. Additionally, the in-cylinder temperature change was not only influenced by the fuel combustion efficiency but also by the fuel substitution rate. The higher the ammonia substitution rate, the greater the evaporation of liquid ammonia, which increases the heat absorption. Both Case 1 and Case 2 showed a decrease in the cylinder temperature peak value as the ammonia substitution rate increased. In both cases, when the ammonia substitution rate exceeded 70%, the temperature curve changed significantly, and the heat deficit from ammonia blending combustion was offset by the combustion benefits of the high-pressure direct injection fuel method. The in-cylinder temperature changes for different ammonia blending ratios under the two injection strategies are shown in Figure 7. Compared to the original engine model, the peak in-cylinder average temperature for

the 50% ammonia substitution rate condition in Case 1 and the 20% ammonia substitution rate condition in Case 2 were 93.89 K and 105.11 K higher, respectively. A higher in-cylinder average temperature typically accompanied the formation of more thermally-formed NOx. The temperature field variations are shown in Figure 8.

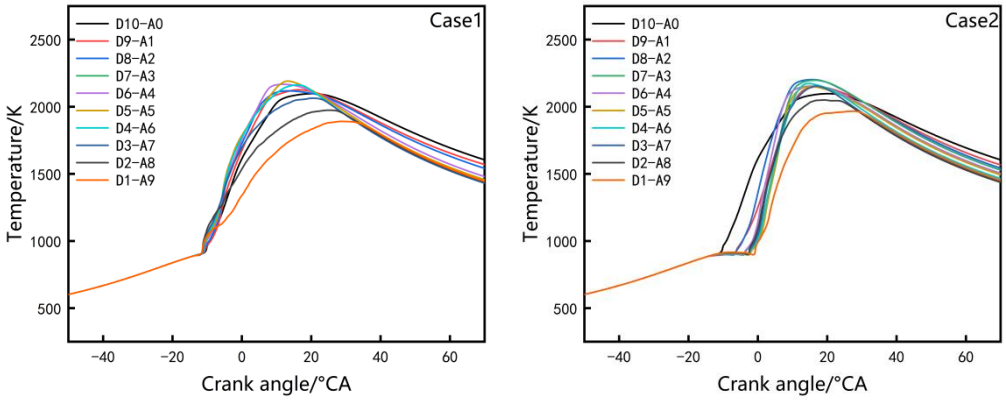

Figure 7. Changes in the cylinder temperature of different diesel/ammonia ratios under the two injection schemes.

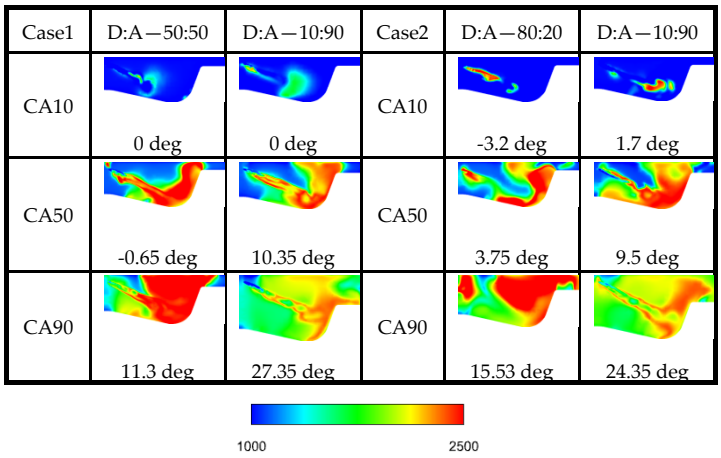

Figure 8. In-cylinder temperature field.

It is worth noting that in Case 1, the fuel injection sequence adopted a diesel-first strategy, where the flame formed by diesel ignition contacted the liquid ammonia jet, igniting the liquid ammonia. Although ammonia has a high latent heat of vaporization, due to the high-pressure injection strategy and the timing of ammonia fuel injection, the ammonia fuel was directly ignited by the flame already formed in the combustion chamber as soon as it entered, especially in the cases with low ammonia substitution rates, where the diesel injection duration fully covered the ammonia injection duration. As a result, liquid ammonia hardly had a chance to evaporate, and its evaporation had little impact on combustion parameters. Since ammonia's vaporization latent heat and autoignition temperature are much higher than those of diesel, in Case 2, the injection strategy was to inject ammonia first. After ammonia mixed with the air inside the cylinder, diesel fuel was injected to ignite it, displaying characteristics of premixed combustion. The inflection point of the in-cylinder temperature curve was delayed with an increase in the ammonia blending ratio and the lag in the diesel injection timing.

3.3. Effect of Different Mixing Ratios on NOx Emission

The total NOx emissions consisted of two parts: one was the high-temperature NOx generated from nitrogen and oxygen in the air under high temperature and pressure, and the other was the fuel-based NOx generated from incomplete combustion of the substitute fuel, ammonia [35]. In most cases with higher substitution ratios, Case 2 exhibited higher in-cylinder temperatures than the same conditions in Case 1. The longer the high-temperature duration, the more high-temperature NOx was produced. The fuel-based NOx generated by ammonia combustion was influenced by the equivalence ratio and temperature, with its formation mechanism being extremely complex. In the low ammonia substitution rate conditions of both Case 1 and Case 2, there may be a balance between the reduction of high-temperature NOx and the increase in fuel-based NOx, causing little fluctuation in the total NOx emissions. After the ammonia substitution rate exceeded 70%, the total NOx emissions decreased. In all cases, as the combustion duration ended and the in-cylinder temperature started to drop, with an increase in the injected ammonia fuel, more liquid ammonia acted as a reducing agent, reacting with NOx in the cylinder and significantly reducing NOx overall. Observing the reduction magnitude and the final total NOx emissions of both schemes, the diesel-first injection method has a clear advantage. Even though Case 2 demonstrated more stable engine performance indices and higher thermal efficiency compared to Case 1, it was often accompanied by more NO and NO_2 emissions. As shown in Figure 9, compared to the original model, the total NOx emissions in Case 1 decreased by 36.6% and 71.5% at 80% and 90% ammonia substitution rates, respectively. Under the same conditions, the total NOx emissions in Case 2 decreased by 28.7% and 63.5%. Furthermore, since ammonia does not carry carbon atoms, ammonia combustion does not produce carbon-containing substances, leading to minor fluctuations in soot emissions at low ammonia substitution rates. As the ammonia substitution rate increased, soot emissions in both Case 1 and Case 2 decreased significantly (Figure 9). Using ammonia as a substitute fuel provides a significant advantage in reducing soot emissions.

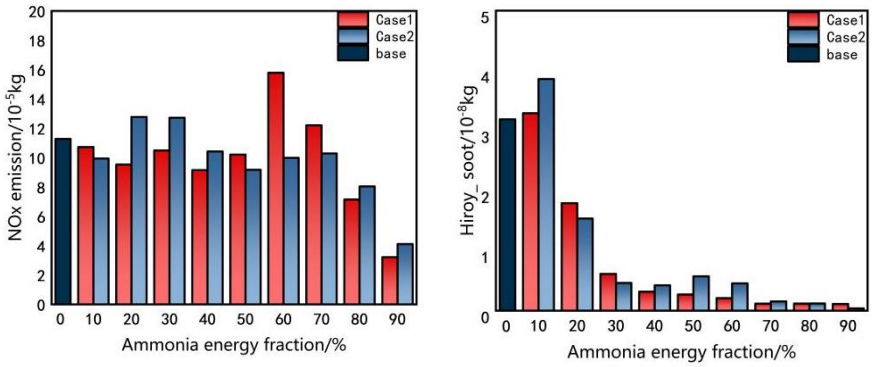

Figure 9. The effect of different diesel/ammonia ratios on the total nitrogen oxide emission and soot changes under the two injection schemes.

From the overall analysis of the components of NOx (Figure 10), NO occupied the largest proportion, and as the main component of NOx, the trend of NO emissions was essentially the same as the overall trend of NOx emissions. Therefore, to control the overall NOx emissions, it is necessary to achieve the highest possible NO reduction rate. There are four main reaction paths for the reduction of NO, as follows:

1. $NH_2 + NO = NNH + OH$;
2. $NH_2 + NO = N_2 + H_2O$;
3. $NH + NO = N_2O + H$; and

4. $N + NO = N_2 + O$.

According to the study by Miller et al. [36], the high-temperature non-catalytic selective reduction of NOx occurs only within a narrow temperature range, typically between 1000 K and 1400 K. Below 1000 K, the reduction rate slows down, with the reduction process being most effective at around 1250 K. Above 1500 K, it may have the opposite effect. At lower temperatures, NO can easily undergo a reduction reaction with NH_2, and as the temperature increases, the concentration of OH and O rises. This causes reaction 5, $NH_2 + O = HNO + H$, to compete with reactions 1 and 2 for NH_2, leading to the decomposition of HNO. The reaction paths change, mainly as follows:

6. $HNO + OH = H_2O + NO$, and

7. $HNO + NH_2 = NH_3 + NO$, both leading to the formation of NO. Therefore, when the temperature is sufficiently high, its oxidation process becomes the dominant reaction process, and NO, the main component of NOx, will not only fail to reduce but will also further precipitate, ultimately leading to an increase in NOx concentration. By analyzing slices based on the CA10 and CA50 moments of the engine's accumulated heat release, as well as the peak moments of each component's concentration, the variation trend of nitrogen oxides in the engine cylinder was observed. The molar mass distribution characteristics of nitrogen oxides are shown in Figure 11. The evolution of NO and N_2O showed opposing trends. NO was primarily distributed in the high-temperature region of the cylinder, and its distribution characteristics were closely related to higher-temperature environments and OH. NO_2 and N_2O were mainly distributed in the low-temperature region of the cylinder. However, NO_2 mainly concentrated in the low-temperature, oxygen-rich region, while N_2O was found in low-temperature, oxygen-rich, and fuel-rich regions.

In the combustion process of dual-fuel engines, the generation of nitrogen oxides (NOx) is influenced by coupling effects. Comparing the corresponding ammonia replacement ratio scenarios under both Case 1 and Case 2, it was expected that Case 1 would exhibit better reduction effects and lower final NOx emissions. This is because, in the Case 2 scenario, part of the ammonia fuel has already entered the cylinder before ignition, meaning that less ammonia fuel is available for the reduction reaction compared to Case 1 under the same ammonia replacement ratios. Based on the simulation results, the major NOx components in both scenarios were analyzed using the generation concentration coordinates at different crank angles (with a magnification applied to show the changes in important components like NO_2 and HNO). As shown in Figure 12, for the three high ammonia replacement scenarios in Case 1 and the 80% and 90% ammonia replacement scenarios in Case 2, the molar fraction of NO, the main component of NOx, exhibited two distinct phases. The first peak corresponded to the NO generated during the dual-fuel combustion process. The first inflection point represented the moment when ammonia fuel was injected into the combustion chamber, and the reduction reaction began, leading to a decrease in NO. However, at this point, ammonia combustion also occurred, and NO concentration increased again. After all fuel injection was completed, the concentrations of NO and N_2O gradually stabilized after oscillating. It can also be observed that the concentration of NO_2 decreased. The formation of NO_2 was more sensitive to changes in the cylinder temperature, showing significant variations before and after the start and end of high-temperature combustion in the low-temperature region. Compared to the NO generated in high-temperature environments, NO_2 tended to form earlier, before NO, as the cylinder temperature rose. In Case 1, the reduction reaction began gradually when the ammonia replacement ratio exceeded 70%. In scenarios with a higher ammonia replacement ratio, the cylinder temperature gradually decreased, and the total NOx emissions decreased as well. Furthermore, the use of a post-injection ammonia strategy allowed more NH_i to participate in the reduction reaction in

the low-temperature region after the average cylinder temperature dropped to 1500 K near the end of the combustion process.

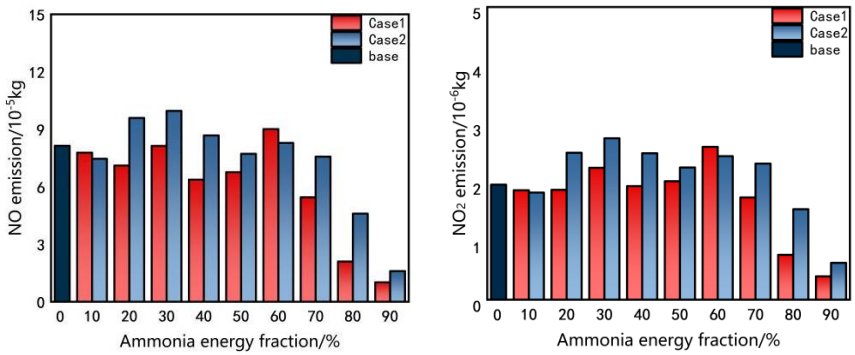

Figure 10. NO/NO_2 emissions.

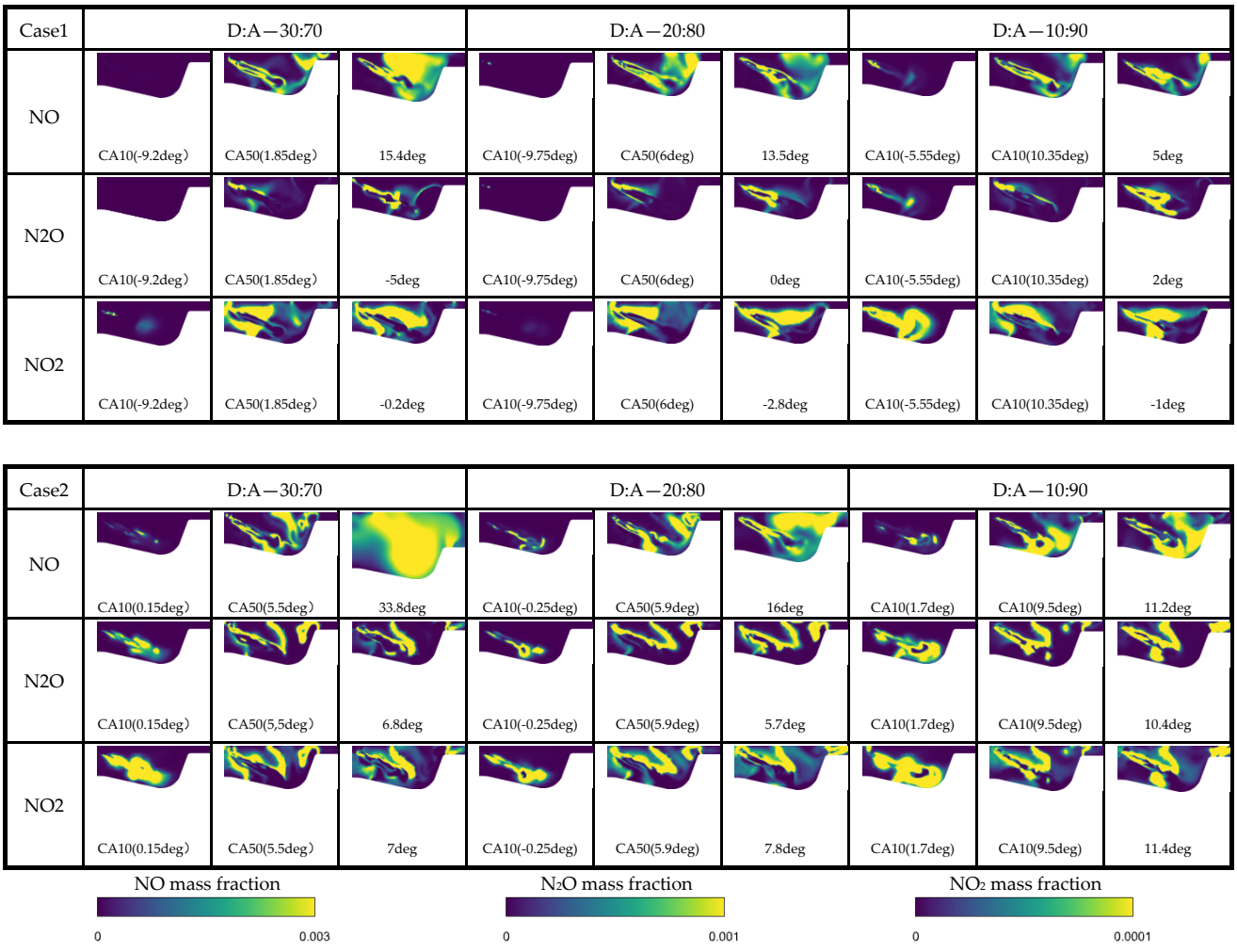

Figure 11. Change in the mass fraction of the main components of nitrogen oxides in the cylinder.

In the Case 2 scenario, the reduction reaction was less noticeable under high ammonia replacement ratios. Due to the ammonia pre-injection strategy, most of the ammonia fuel was consumed before it could participate in the reduction reaction. However, in the 90% ammonia replacement scenario, due to the specific injection strategy, the main combustion duration (from CA10 to CA90) ended around 24.35 degrees, while the ammonia fuel injection continued, allowing the new liquid ammonia to contribute to the reduction reaction and significantly reduce NOx emissions. Additionally, it can be

observed that NH_i had a more pronounced inhibitory effect on NO compared to NO and N_2O. This is largely because the concentration of NO was relatively high, making it more likely to react with the reductant. In contrast, the concentrations of NO_2 and N_2O were lower, and their conversion to harmless substances like N_2 requires multiple reaction steps. Therefore, the reduction and harmless treatment effects of NO_2 and N_2O were less significant compared to NO.

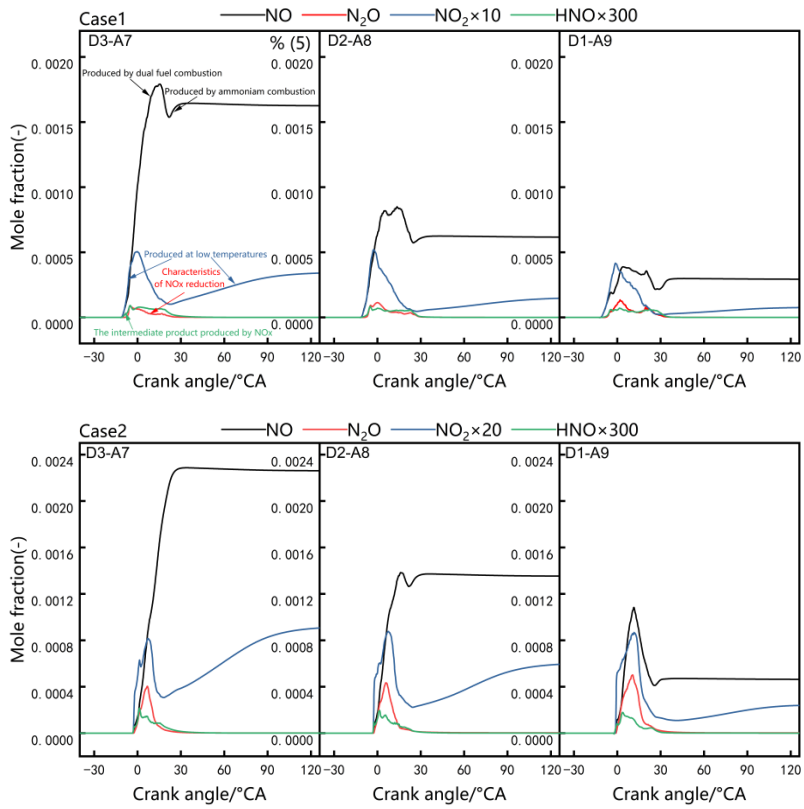

Figure 12. In-cylinder NOx mole fraction.

3.4. In-Cylinder OH Distribution Under Different Ammonia Substitution Rates

The hydroxyl (OH) radical is an important intermediate product in the fuel oxidation process. Both n-heptane, representing diesel fuel, and ammonia fuel continuously generate OH during the combustion reaction. For diesel fuel, n-heptane undergoes low-temperature reactions before combustion, where the C-H bonds and the O-O bonds in the oxygen from the air tend to break more easily. This leads to hydrogen abstraction and oxygen addition, forming different isomers. As the reaction proceeds, n-heptane undergoes isomerization, generating and accumulating large amounts of OH. Additionally, n-heptane also influences the formation and reduction of NO, as the C-H radicals produced by n-heptane have a positive reduction effect on NO.

Similar to n-heptane, ammonia also generates OH continuously during combustion reactions and reacts intensely with OH. In ammonia fuel, the conversion of NH_3 to NH_i involves a dehydrogenation process. The main reaction for NOx reduction to N_2 is NH_2 + NO. To ensure the continuity of this reaction, it is essential to continuously generate OH and O, which mainly come from the following reactions:

1. $NH_2 + NO = NNH + OH$;
2. $NNH + NO = N_2 + HNO$
3. $HNO + M = H + NO + M$.

In reaction 3, the H atom reacts with O_2 in the exhaust gas to form OH. As combustion continues, the temperature inside the cylinder rises, and the highly active OH generated

from the low-temperature reactions stimulates the fuel to continue burning. At this point, n-heptane will stop undergoing dehydrogenation and oxygen addition in the low-temperature reaction path and shift to the high-temperature reaction phase. In this phase, n-heptane directly cracks into short-chain alkanes, generating large amounts of OH radicals and further promoting high-temperature reactions, leading to intense combustion.

To explore the distribution of OH radicals and the evolution of temperature and emissions, it is necessary to analyze the OH distribution from ignition to combustion. Figure 13 shows the vertical slice analysis of the OH formation and main diffusion stages at CA10 and CA50 moments for high ammonia replacement ratios under both Case 1 and Case 2. OH distribution reflected the combustion reaction speed, which correlated with the temperature of the corresponding regions. By observing the distribution of OH formation, we can predict the temperature distribution within the cylinder. At CA10, the OH generation in both Case 1 and Case 2 was located outside the spray near the nozzle. By CA50, OH moved toward the spray end, then moved inward toward the piston wall and subsequently spread outward across the combustion chamber. This analysis provides insights into the ignition and combustion progression and the mechanisms behind emissions formation.

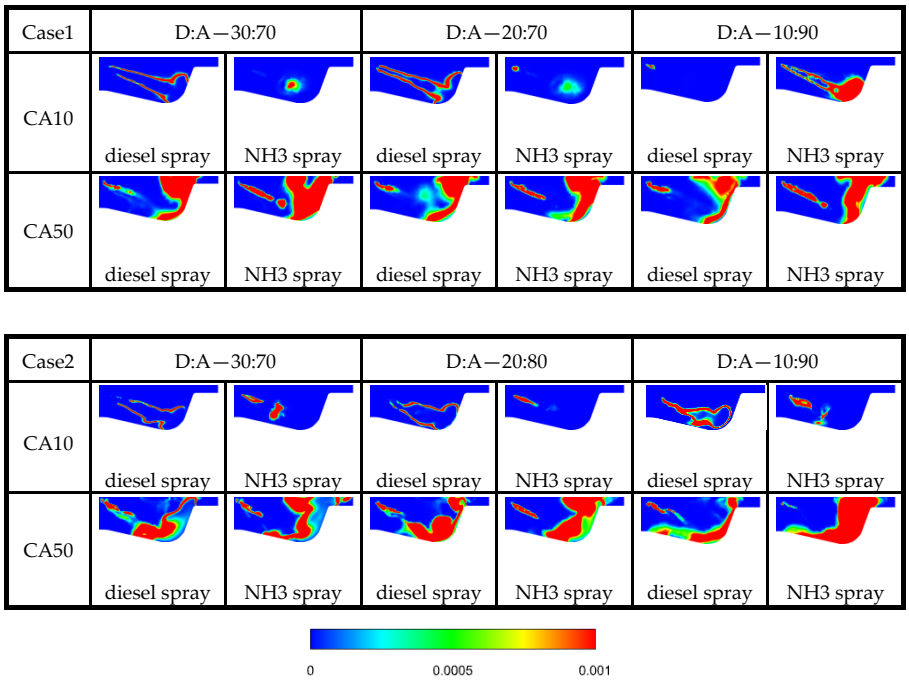

Figure 13. In-cylinder OH distribution at different stages.

3.5. Effect of Different Mixing Ratios on Greenhouse Gas Emissions

CO_2 emissions are primarily influenced by the combustion of diesel, and n-heptane, which represents diesel in this study, is the only component in the dual-fuel mixture that contains carbon. From the decreasing trend in CO_2 emissions shown in Figure 13, it can be concluded that ammonia as a substitute fuel demonstrated excellent zero-carbon combustion performance. As the ammonia replacement rate increased, the final greenhouse gas emissions gradually decreased, as depicted in Figure 14.

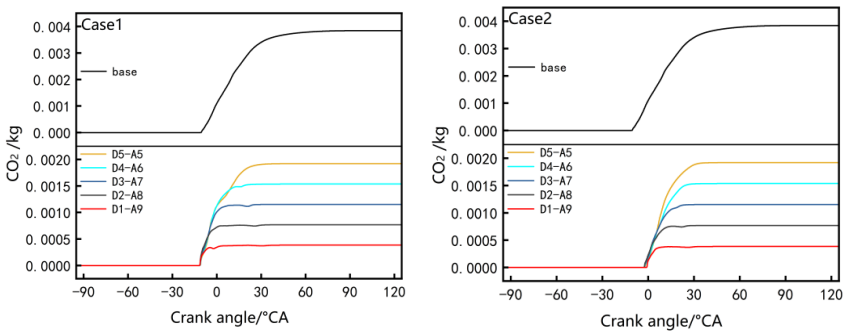

Figure 14. Greenhouse gas emissions.

N_2O has a more significant impact on the greenhouse effect compared to CO_2, with a global warming potential 300 times greater than that of CO_2 [37,38]. The production of N_2O involves a complex multi-reaction process, primarily associated with ammonia combustion and the reduction of NO and NO_2, which results in the formation of this important byproduct. OH and NO are mainly produced in high-temperature combustion regions, while N_2O is mainly produced in low-temperature combustion areas. The distribution of N_2O is related to the environmental temperature and equivalence ratio [39,40]. The evolution of N_2O and NO follows opposing trends. This phenomenon can be attributed to the reduction of NO by NH, which leads to the formation of N_2O. NH_2 and NH species also promote the conversion of NO_2 to NO and N_2O through reactions like:

1. $NO_2 + NH_2 = NO + H_2NO$;
2. $NO_2 + NH = NO + HNO$;
3. $NH_2 + NO_2 = N_2O + H_2O$;
4. $NH + NO_2 = N_2O + OH$.

Additionally, NO, NO_2 and N_2O can interconvert, as seen in reactions like:

1. $N_2O + O = 2NO$;
2. $N_2O + NO = N_2 + NO_2$.

The free radicals OH, O, and H produced by high-pressure dual-fuel injection strategies react with N_2O, forming reactions like:

1. $N_2O + OH = N_2 + HO_2$;
2. $N_2O + O = N_2 + O_2$;
3. $N_2O + H = N_2 + OH$.

In Case 1, the high-pressure injection strategy ensured that liquid ammonia ignited quickly once entering the combustion chamber, overcoming ammonia's slow flame speed and allowing for more complete combustion. Only a small portion of ammonia formed by liquid ammonia evaporation remained incompletely combusted, resulting in minimal N_2O formation. As shown in Figure 15, in Case 2, the strategy of injecting ammonia first led to the formation of some premixed gases, which increased the N_2O emissions compared to Case 1 under the same conditions. Even after multiplying N_2O emissions for comparison, the emissions were still three orders of magnitude lower than CO_2 emissions. Therefore, controlling CO_2 emissions remains a priority for greenhouse gas reduction. Furthermore, if the diesel-first injection strategy from Case 1 is used, the overall N_2O emissions can still be well controlled.

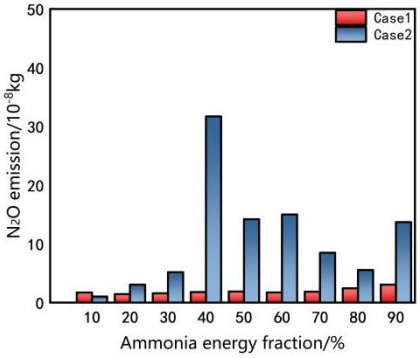

Figure 15. N_2O emissions.

4. Conclusions

This study utilized numerical simulation combined with the selective non-catalytic reduction (SNCR) reaction mechanism to analyze a diesel/ammonia dual-fuel high-pressure direct injection engine. By comparing different ammonia fuel durations and substitution ratios for each pre-set engine operating condition, the following conclusions were drawn:

1. Compared to the intake manifold pre-mixed dual-fuel combustion mode, the high-pressure direct injection dual-fuel mode offers higher fuel supply efficiency while avoiding the loss of ammonia fuel due to wall attachment in the intake manifold section after injection. Additionally, this injection strategy is more flexible, allowing for a precise and rapid injection of ammonia fuel. By adjusting the fuel injection timing and spray angle, combustion can be more accurately controlled. The change in injection timing and the dual-fuel injection strategy at low ammonia substitution rates shorten the total fuel injection duration, with more fuel being injected before the engine reaches the top dead center (TDC). As the engine moves toward TDC, the combustion chamber volume decreases, so the earlier the fuel participates in combustion, the greater its contribution to cylinder pressure and temperature increase. By analyzing the total heat release and cylinder volume change curves, it can be seen that stable combustion was achieved even at high ammonia substitution rates. The cylinder pressure and heat release rate curves indicated that the strategy of injecting ammonia first, followed by diesel, exhibited some characteristics of pre-mixed combustion.
2. When using the diesel/ammonia high-pressure injection strategy for combustion, NOx emissions were significantly reduced in both pre-set cases during high ammonia substitution conditions. By analyzing each set of conditions for the sequence of fuel injection, it was found that when the ammonia substitution rate exceeded 70%, NOx emissions began to decrease. As the ammonia substitution rate continued to increase, the injection duration also increased. After the main combustion period ended, the dehydrogenated products (NH_i) of the continuously injected ammonia fuel reduced the majority of NOx, particularly NO, when the cylinder temperature dropped to 1500 K. Under the condition of limiting nozzle size and injection pressure, the strategy of injecting diesel first and then ammonia allowed more ammonia to participate in the subsequent selective catalytic reduction (SCR) reaction, significantly reducing the final NOx emissions.
3. The high-temperature non-catalytic selective reduction of NOx occurs within a narrow temperature range. If the temperature is too high or too low, NOx reduction becomes either ineffective or counterproductive. When the temperature exceeds this range, the chemical reaction pathways change, and NO is not reduced, while a large

amount of NO is released, further increasing NOx emissions. Based on the distribution characteristics of OH and nitrogen oxides in the cylinder, it was found that OH, which is crucial for promoting ammonia fuel reaction pathways, had a distribution closely related to the cylinder temperature. The generation and accumulation of OH was indicative of high-temperature reactions. The trends of NO and N_2O evolution within the cylinder were opposite; NO was primarily generated in high-temperature regions, while NO_2 and N_2O were mainly produced in low-temperature regions. Additionally, NO_2 was more sensitive to ambient temperature, with significant changes before and after the engine's combustion duration.

4. After adopting the diesel/ammonia high-pressure injection strategy, the primary greenhouse gas component, CO_2, begins to decrease as the ammonia substitution rate increases. Since ammonia does not contain carbon atoms, increasing its substitution rate leads to a reduction in carbon components (such as soot) and carbon-containing products in the final emissions, highlighting ammonia's advantage as a substitute fuel. For another greenhouse gas component, N_2O, its emissions can be effectively controlled by adjusting the fuel injection strategy.

Author Contributions: Project administration and resources, Z.W.; writing—original draft preparation, R.L.; writing—review and editing, Software, J.Z.; Visualization, Validation, Z.F. All authors have read and agreed to the published version of the manuscript.

Funding: Supported by the National Key R&D Program of China (Grant No. 2022YFB4300701, Dec. 2022–Nov. 2026).

Data Availability Statement: No additional data are available.

Acknowledgments: The author appreciates the support and assistance of the Carbon Emission Control Laboratory of Shanghai Maritime University.

Conflicts of Interest: The authors declare no conflicts of interest.

References

1. Kitano, M.; Inoue, Y.; Yamazaki, Y.; Hayashi, F.; Kanbara, S.; Matsuishi, S.; Yokoyama, T.; Kim, S.W.; Hara, M.; Hosono, H. Ammonia synthesis using a stable electride as an electron donor and reversible hydrogen store. *Nat. Chem.* **2012**, *4*, 934–940.
2. Dimitriou, P.; Javaid, R. A review of ammonia as a compression ignition engine fuel. *Int. J. Hydrogen Energy* **2020**, *45*, 7098–7118.
3. Qiu, Y.; Zhang, Y.; Shi, Y.; Zhang, Y.; Wang, Z.; Lin, H.; Han, D.; Huang, Z. Ammonia fueled engine with diesel pilot ignition: Approach to achieve ultra-high ammonia substitution. *Int. J. Engine Res.* **2024**, *25*, 1751–1763.
4. Liu, X.; Tang, Q.; Im, H.G. Enhancing ammonia engine efficiency through pre-chamber combustion and dual-fuel compression ignition techniques. *J. Clean. Prod.* **2024**, *436*, 140622.
5. Li, T.; Zhou, X.Y. A comparison between low- pressure and high-pressure injection dualfuel modes of diesel-pilot-ignition ammonia combustion engines. *J. Energy Inst.* **2022**, *102*, 362–373.
6. Stephanie, F.; Stephan, G. Investigation of ammonia and hydrogen as CO_2-free fuels for heavy duty engines using a high pressure dual fuel combustion process. *Int. J. Engine Res.* **2020**, *1*, 23–34.
7. Reiter, A.J.; Kong, S.C. Demonstration of compression-ignition engine combustion using ammonia in reducing greenhouse gas emissions. *Energy Fuel* **2008**, *22*, 2963–2971.
8. Reiter, A.J.; Kong, S.C. Combustion and emissions characteristics of compressionignition engine using dual ammonia-diesel fuel. *Fuel* **2011**, *90*, 87–97.
9. Zhang, Z.; Di, L.; Shi, L.; Yang, X.; Cheng, T.; Shi, C. Effect of liquid ammonia HPDI strategies on combustion characteristics and emission formation of ammonia-diesel dual-fuel heavy-duty engines. *Fuel* **2024**, *367*, 131450.
10. Yang, R.; Yue, Z.; Zhang, S.; Yu, Z.; Wang, H.; Liu, H.; Yao, M. A novel approach of in-cylinder NOx control by inner selective non-catalytic reduction effect for high-pressure direct-injection ammonia engine. *Fuel* **2025**, *381*, 133349.

11. Li, Z.; Wang, Y.; Yin, Z.; Gao, Z.; Wang, Y.; Zhen, X. An exploratory numerical study of a diesel/methanol dual-fuel injector: Effects of nozzle number, nozzle diameter and spray spacial angle on a diesel/methanol dual-fuel direct injection engine. *Fuel* **2022**, *318*, 123700.
12. Xu, L.; Chang, Y.; Treacy, M.; Zhou, Y.; Jia, M.; Bai, X.S. A skeletal chemical kinetic mechanism for ammonia/n-heptane combustion. *Fuel* **2023**, *331*, 125830.
13. Xinlei, L.; Sage, K.; Hu, W.; Mingfa, Y,A comparative numerical investigation of reactivity controlled compression ignition combustion using large eddy simulation and reynolds-averaged navier-stokes approaches. *Fuel* **2022**, *257*, 116023.
14. Shi, X.R.; Xiong, Q.; Pan, C.Y.; Liu, L.; Fu, S.Y.; Zhao, J.H. Effect of ammonia energy fraction and injection strategy on the combustion and emission of dual-fuel low-speed engine. *J. Int. Combust. Eng.* **2024**, *42*, 489–498.
15. Han, Z.; Reitz, R.D. Turbulence modeling of internal combustion engines using RNG k-ε models. *Combust Sci. Technol.* **1995**, *106*, 267–295.
16. Dec, J.E.; Reltz, R.D. Comparisons of diesel spray liquid penetration and vapor fuel distributions with in-cylinder optical measurements. *J. Eng. Gas. Turb. Power* **2000**, *122*, 588–595.
17. O'Rourke, P.J.; Amsden, A.A. A spray/wall interaction submodel for the KIVA-3 wall film model. *J. Engines* **2000**, *109*, 281–298.
18. Schmidt, D.P.; Rutland, C.J. A new droplet collision algorithm. *J. Comput. Phys.* **2000**, *164*, 62–80.
19. Han, Z.; Reitz, R.D. A temperature wall function formulation for variable-density turbulent flows with application to engine convective heat transfer modeling. *Int. J. Heat Mass Tran.* **1997**, *40*, 613–625.
20. Senecal, P.K.; Pomraning, E.; Richards, K.J.; Briggs, T.E.; Choi, C.Y.; McDavid, R.M.; Patterson, M.A. Multi-dimensional modeling of direct-injection diesel spray liquid length and flame lift-off length using cfd and parallel detailed chemistry. *J. Engines* **2003**, *112*, 1331–1351.
21. Maroteaux, F.; Saad, C. Combined mean value engine model and crank angle resolved in-cylinder modeling with NOx emissions model for real-time diesel engine simulations at high engine speed. *Energy* **2015**, *88*, 515–527.
22. Li, Z.; Wang, Y.; Yin, Z.; Gao, Z.; Wang, Y.; Zhen, X. Parametric study of a single-channel diesel/methanol dual-fuel injector on a diesel engine fueled with directly injected methanol and pilot diesel, *Fuel* **2021**, *302*, 121156.
23. Fisher, C.J. A study of rich ammonia/oxygen/nitrogen flames. *Combust. Flame* **1977**, *30*, 143–149.
24. Miller, J.A.; Bowman, C.T. Mechanism and modeling of nitrogen chemistry in combustion. *Prog. Energy Combust.* **1989**, *15*, 287–338.
25. Lyon, R.K. The NH3 -NO-O2 reaction. *Int. J. Chem. Kinet.* **1976**, *8*, 315–318.
26. Lee, G.W.; Shon, B.H.; Yoo, J.G.; Jung, J.H.; Oh, K.J. The influence of mixing between NH3 and NO for a De-NOx reaction in the SNCR process. *J. Ind. Eng. Chem.* **2008**, *144*, 457–467.
27. He, X.; Shu, B.; Nascimento, D.; Moshammer, K.; Costa, M.; Fernandes, R.X. Auto-ignition kinetics of ammonia and ammonia/hydrogen mixtures at intermediate temperatures and high pressures. *Combust. Flame* **2019**, *206*, 189–200.
28. Sabia, P.; Manna, M.V.; Cavaliere, A.; Ragucci, R.; de Joannon, M. Ammonia oxidation features in a Jet Stirred Flow Reactor. The role of NH2 chemistry. *Fuel* **2020**, *276*, 118054.
29. Lindstedt, R.; Lockwood, F.; Selim, M. Detailed kinetic modelling of chemistry and temperature effects on ammonia oxidation. *Combust. Sci. Technol.* **1994**, *99*, 253–276.
30. Mei, B.; Zhang, X.; Ma, S.; Cui, M.; Guo, H.; Cao, Z.; Li, Y. Experimental and kinetic modeling investigation on the laminar flame propagation of ammonia under oxygen enrichment and elevated pressure conditions. *Combust. Flame* **2019**, *210*, 236–246.
31. Zhang, X.; Moosakutty, S.P.; Rajan, R.P.; Younes, M.; Sarathy, S.M. Combustion chemistry of ammonia/hydrogen mixtures: Jet-stirred reactor measurements and comprehensive kinetic modeling. *Combust. Flame* **2021**, *234*, 111653.
32. Abián, M.; Benés, M.; De Goñi, A.; Muñoz, B.; Alzueta, M.U. Study of the oxidation of ammonia in a flow reactor. Experiments and kinetic modeling simulation. *Fuel* **2021**, *300*, 979.
33. Mathieu, O.; Petersen, E.L. Experimental and modeling study on the high-temperature oxidation of ammonia and related NOx chemistry. *Combust. Flame* **2015**, *162*, 554–570.
34. Shrestha, K.P.; Seidel, L.; Zeuch, T.; Mauss, F. Detailed kinetic mechanism for the oxidation of ammonia including the formation and reduction of nitrogen oxides. *Energy Fuels* **2018**, *32*, 10202–10217.
35. Kobayashi, H.; Hayakawa, A.; Somarathne, K.K.A.; Okafor, E.C. Science and technology of ammonia combustion. *Proc. Combust. Inst.* **2019**, *37*, 109–133.
36. Miller, J.A.; Branch, M.C.; Kee, R.J. A chemical kinetic model for the selective reduction of nitric oxide by ammonia. *Combust. Flame* **1981**, *43*, 81–98.

37. Chiong, M.C.; Chong, C.T.; Ng, J.H.; Mashruk, S.; Chong, W.W.F.; Samiran, N.A.; Mong, G.R.; Valera-Medina, A. Advancements of combustion technologies in the ammonia-fuelled engines. *Energy Convers. Manag.* **2021**, *244*, 114460.
38. Yousefi, A.; Guo, H.; Dev, S.; Liko, B.; Lafrance, S. Effects of ammonia energy fraction and diesel injection timing on combustion and emissions of an ammonia/diesel dual-fuel engine. *Fuel* **2022**, *314*, 122723.
39. Duynslaegher, C.; Jeanmart, H.; Vandooren, J. Flame structure studies of premixed ammonia/hydrogen/oxygen/argon flames: Experimental and numerical investigation. *Proc. Combust. Inst.* **2009**, *32*, 1277–1284.
40. Nakamura, H.; Hasegawa, S.; Tezuka, T. Kinetic modeling of ammonia/air weak flames in a micro flow reactor with a controlled temperature profile. *Combust. Flame* **2017**, *185*, 16–27.